

Surface response of a polymer network: Semi-infinite network

Chen Bar-Haim* and Haim Diamant*

*Raymond & Beverly Sackler School of Chemistry, Tel Aviv University, Tel Aviv 6997801,
Israel*

E-mail: chentush@gmail.com; hdiamant@tau.ac.il

Abstract

We study theoretically the surface response of a semi-infinite viscoelastic polymer network using the two-fluid model. We focus on the overdamped limit and on the effect of the network's intrinsic length scales. We calculate the decay rate of slow surface fluctuations, and the surface displacement in response to a localized force. Deviations from the large-scale continuum response are found at length scales much larger than the network's mesh size. We discuss implications for surface scattering and microrheology. We provide closed-form expressions that can be used for surface microrheology—the extraction of viscoelastic moduli and intrinsic length scales from the motions of tracer particles lying on the surface without doping the bulk material.

Introduction

Surfaces of materials exhibit distinctive behaviors compared to the bulk.¹ This applies, in particular, to the deformations of liquid and solid surfaces in response to stresses and thermal fluctuations, as has been studied for many years. Important examples are capillarity of liquid surfaces² and Rayleigh waves on solid surfaces.³ In the present work we consider the surfaces of materials whose response lies in-between these two limits, i.e., viscoelastic media made of both fluid and solid components.

Surface waves in polymer solutions and gels have been thoroughly studied using various light scattering and mechanical excitation techniques.^{4–8} (See a recent review in ref 9.) A characteristic feature of these experiments is the crossover from capillary (surface-tension-dominated) waves to Rayleigh (elasticity-dominated) waves with decreasing frequency or increasing concentration. The prevalent theory for the dispersion relation of these waves on the surface of a semi-infinite viscoelastic medium is by Harden, Pleiner, and Pincus.^{10–12} Its validity has been confirmed by the experiments mentioned above. Extensions have been developed for more complicated scenarios, such as the existence of an adsorbed layer of

different mechanical properties,^{13,14} and a supported film of finite thickness.¹⁵ All these models have considered the strong coupling limit where the viscous and elastic components move together as a structureless medium.

Our focus here is different. We are interested in the effect of the intrinsic length scales characterizing a structured fluid on its surface response, and how these characteristics can be extracted from surface measurements. This is motivated by recent studies, which have revealed a dynamic length scale intermediate between the material's static correlation length and the limit of structureless bulk response.^{16–19} The intermediate length scale was found to be associated with a distinctive mechanical response. Therefore, we extend earlier theories for the relaxation of liquid and solid surfaces,²⁰ as well as the response of the surface to a localized force,³ to the case of a structured viscoelastic medium described by the two-fluid model.^{18,21–26}

The present work is particularly relevant to the study of the mechanical response of soft materials. Viscoelastic response is commonly studied by rheometers,²⁷ but this macroscopic technique cannot be applied directly to the surface of the material. (Quasi-two-dimensional rheometers were developed for thin layers lying at fluid interfaces.²⁸) One alternative is to extract the viscoelastic moduli from the dispersion relation of surface waves.⁹ Another relevant technique is microrheology, where the viscoelastic moduli are extracted from the motions of tracer particles.^{29–31} This technique has been applied primarily in the bulk. It may be advantageous in certain cases to obtain bulk microrheological properties from the motions of tracer particles positioned on the surface of a material, without doping the bulk.^{32–37} As far as we know, there is no theory to accompany such experiments, which considers the material as a structured fluid.

The article is organized as follows. After presenting the model, we divide the results into two parts. The first concerns the overdamped dispersion relation (decay rate) of fluctuation modes on the surface of a viscoelastic medium. In the second part we study the surface deformation of such a medium in response to a localized force. Finally, we discuss the findings and their potential usage in experiments.

Model

We consider a semi-infinite polymer solution, occupying the region $z < 0$. We use the two-fluid model^{18,21–26} to describe the structured medium. The model has two components — a semi-dilute polymer network, structurally characterized by a correlation length ξ , and a structureless solvent. See the schematic illustration in Figure 1. The network is described as a (visco)elastic medium, whose deformation is defined by a displacement field $\mathbf{u}(\mathbf{r}, \omega)$, which is a function of position $\mathbf{r} = (\boldsymbol{\rho}, z)$ and frequency ω . The corresponding stress tensor is

$$\sigma_{ij}^{(u)} = 2G [u_{ij} - (u_{kk}/3) \delta_{ij}] + K u_{kk} \delta_{ij}, \quad (1)$$

where $u_{ij} \equiv (\partial_i u_j + \partial_j u_i)/2$ is the network's strain tensor, and G and K its shear and compression moduli, which may be frequency-dependent. We distinguish between the shear modulus of the *bare* network, $G(\omega)$, and the modulus of the bulk material, $G_b(\omega)$, to be presented below. The solvent is described as a viscous incompressible fluid, having a flow velocity field $\mathbf{v}(\mathbf{r}, \omega)$, pressure field $p(\mathbf{r}, \omega)$, and the stress tensor

$$\sigma_{ij}^{(v)} = -p \delta_{ij} + 2\eta v_{ij}, \quad (2)$$

where $v_{ij} \equiv (\partial_i v_j + \partial_j v_i) / 2$ is the fluid's strain-rate tensor, and η its shear viscosity.

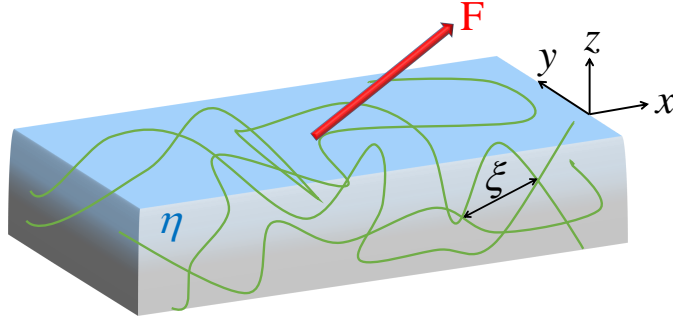


Figure 1: Schematic view of the system and its parameters.

The two components are coupled through mutual friction characterized by a coefficient Γ . In the present work, we focus on the overdamped response of a surface. Thus, neglecting inertia, we write the governing equations for the three fields $(\mathbf{u}, \mathbf{v}, p)$ as follows:

$$0 = \nabla \cdot \sigma_{ij}^{(u)} - \Gamma (i\omega \mathbf{u} - \mathbf{v}), \quad (3)$$

$$0 = \nabla \cdot \sigma_{ij}^{(v)} - \Gamma (\mathbf{v} - i\omega \mathbf{u}), \quad (4)$$

$$0 = \nabla \cdot \mathbf{v}. \quad (5)$$

The first two equations, together, reflect the conservation of momentum in the composite material. The third accounts for the conservation of mass which, in the assumed limit of a semi-dilute solution, is dominated by the incompressible solvent. The frictional force density in eqs 3 and 4 is proportional to the local relative velocity of the two components, thus maintaining overall Galilean invariance. The friction coefficient Γ is related to the correlation length ξ as $\Gamma \sim \eta/\xi^2$.¹⁰

Equations 1–5 are supplemented by the following boundary conditions. (a) Far deep into the medium both components are stationary,

$$\mathbf{u}(\boldsymbol{\rho}, z \rightarrow -\infty) = \mathbf{v}(\boldsymbol{\rho}, z \rightarrow -\infty) = \nabla p(\boldsymbol{\rho}, z \rightarrow -\infty) = 0. \quad (6)$$

(b) At the surface the two components move together,

$$i\omega \mathbf{u}(\boldsymbol{\rho}, z = 0) = \mathbf{v}(\boldsymbol{\rho}, z = 0). \quad (7)$$

This boundary condition implies strong coupling between the two components at the surface. We discuss it further in the Discussion section, where we also offer an alternative if this assumption should be relaxed. (c) At the surface the total stress in the medium balances

the other surface forces,

$$\sigma_{iz}^{(u)}(\boldsymbol{\rho}, z=0) + \sigma_{iz}^{(v)}(\boldsymbol{\rho}, z=0) = f_i - \gamma \nabla_\rho^2 u_z \delta_{iz}. \quad (8)$$

Here, we have included an external surface force density \mathbf{f} and a restoring force due to the surface tension γ , where ∇_ρ^2 is a two-dimensional laplacian. Equations 1–8 define our model.

It is convenient to introduce the following parameters to make the physics more transparent:

$$\eta_b \equiv G / (i\omega) + \eta, \quad (9)$$

$$\xi \equiv \left(\frac{G\eta}{i\omega\Gamma\eta_b} \right)^{1/2}, \quad (10)$$

$$\lambda \equiv \left(\frac{K + 4G/3}{i\omega\Gamma} \right)^{1/2} = \left[\frac{2(1-\nu)\eta_b}{1-2\nu} \frac{1}{\eta} \right]^{1/2} \xi, \quad (11)$$

where $\nu \equiv (3K - 2G)/[2(3K + G)]$ is the network's Poisson ratio. The bulk viscosity $\eta_b(\omega)$ characterizes the large-scale shear response of the two-component medium. We note that it emerges from the smaller-scale parameters, G and η , and is complex in principle, containing both elastic and viscous contributions. The material's bulk shear modulus is simply $G_b = i\omega\eta_b$. The correlation length ξ is another emergent property. It is known to coincide (up to a factor of order unity) with the network's mesh size.^{16,17} It also characterizes the spatial decay of transverse (shear) stresses due to the friction between the two components and, therefore, decreases with increasing Γ . An important conclusion is that any experiments tapping into the internal structure of the complex fluid require a finite network-solvent friction Γ to be accounted for by the two-fluid model. For the low frequencies assumed here, we expect a small contribution to G_b from the solvent, i.e., $G_b(\omega) \simeq G(\omega)$; then, $\xi^2 \simeq \eta/\Gamma$ is insensitive to frequency, as physically expected and as noted above. Another length, $\lambda > \xi$, is related to the compressive (longitudinal) response of the polymer component. Typically $\eta_b \gg \eta$ and, hence, $\lambda \gg \xi$. Moreover, λ diverges in the limit of an incompressible network ($\nu \rightarrow 1/2$ or $K \rightarrow \infty$). Note that the continuum theory that we employ is valid only over distances much larger than ξ .

The surface tension together with the correlation length of the structured fluid introduces a characteristic relaxation time,

$$\Omega^{-1} \equiv \frac{\eta\xi}{\gamma}. \quad (12)$$

The surface tension is associated also with an elasto-capillary length,

$$l_{ec} \equiv \frac{\gamma}{i\omega\eta_b} = \frac{\gamma}{G_b} \quad (13)$$

Results

Structure of the general solution

Applying a Fourier transform, $\tilde{g}(\mathbf{q}, \omega) \equiv \int g(\boldsymbol{\rho}, \omega) e^{-i\mathbf{q}\cdot\boldsymbol{\rho}} d^2\rho$, to all the fields in eqs 1–8 turns those partial differential equations into ordinary differential ones, dependent on z . The general solution³⁸ is a composition of six modes, $e^{\pm\kappa_n z}$, $n = 1, 2, 3$, where

$$\kappa_1 = q, \quad \kappa_2 = \sqrt{q^2 + \xi^{-2}}, \quad \kappa_3 = \sqrt{q^2 + \lambda^{-2}}. \quad (14)$$

The general solution for the network displacement $\mathbf{u}(\mathbf{q}, \omega)$ contains all six modes, that for the solvent velocity $\mathbf{v}(\mathbf{q}, \omega)$ four modes ($n = 1, 2$), and the one for the solvent pressure $p(\mathbf{q}, \omega)$ four modes ($n = 1, 3$). Thus, altogether, the general solution contains 14 amplitudes. These are determined by the thirteen boundary conditions defined in eqs 6–8, plus the incompressibility constraint of eq 5. After omitting the three modes which diverge at $z \rightarrow -\infty$, we are left with three decaying modes, whose “penetration depths” are defined in eq 14, and seven amplitudes to be determined. For a large-wavelength surface perturbation ($q \rightarrow 0$), one of the modes ($n = 1$) extends throughout the medium, whereas the other two remain localized at the surface, with penetration depths ξ and λ . We note that the two surface-localized modes ($n = 2, 3$) differ from the ones discussed in ref 39 in that they depend on the intrinsic lengths ξ and λ .

Dispersion relation of overdamped surface fluctuations

To obtain the decay rate of the overdamped surface fluctuations as a function of wavevector q , we set $\mathbf{f} = 0$ in the surface stress, eq 8, and look for nontrivial solutions for \mathbf{u} , \mathbf{v} and p . This amounts to the requirement that the matrix corresponding to the linear equations for the seven amplitudes should have a zero determinant. The resulting equation gives the dispersion relation, $-i\omega(q)$.

The full equation is complicated and can be found in the supplemental material.⁴⁰ It has two linear asymptotes, at small and large q , with a crossover at $q \sim \lambda^{-1}$,

$$-i\omega = \begin{cases} \frac{\gamma q}{2\eta_b}, & q \ll \lambda^{-1}, \\ \frac{\gamma q}{2\eta_b} \frac{\beta^2}{\beta^2 - 1}, & \lambda^{-1} \ll q \ll \xi^{-1}, \end{cases} \quad (15)$$

where

$$\beta(\nu) = [2(1 - \nu)/(1 - 2\nu)]^{1/2} \geq 2/\sqrt{3}. \quad (16)$$

(The lower bound for β comes from the validity range of the Poisson ratio, $-1 \leq \nu \leq 1/2$.) The small- q limit corresponds to the bulk response of the medium and coincides with the dispersion relation for overdamped surface fluctuations of a viscous fluid whose viscosity is replaced by η_b . The other asymptote describes the dispersion relation in the intermediate region $\lambda^{-1} \ll q \ll \xi^{-1}$.

Since the bulk viscosity $\eta_b(\omega)$ is a function of ω , the equation that we obtain for the

dispersion relation, along with its asymptotes eq 15, in fact, is an implicit equation for the rate, which can be solved only if $\eta_b(\omega)$ is known. We give three simple limits where the dispersion relation can be obtained explicitly.

The first simple case holds if η_b changes slowly with ω over the range of q of interest, and can be assumed constant. The full solution in this limit is represented by the solid curve in Figure 2. The two asymptotes are presented as well. The gap between the two asymptotes depends on the compressibility of the bare polymer network, and vanishes in the limit of incompressibility. For the curve in Figure 2 we have chosen an unrealistically small value for the Poisson ratio ($\nu = 0.1$) to demonstrate the gap between the two asymptotes (amounting in this case to a factor of about 3). For a much less compressible network, the gap is smaller but still not negligible; for example, for a realistic value of $\nu = 0.4$ the difference between the asymptotes is by a factor of 1.2.

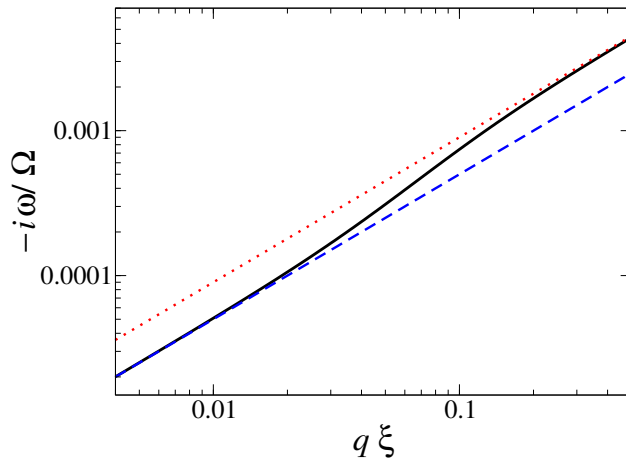


Figure 2: Normalized rate $-i\omega(q)$ as a function of normalized wavevector. Once normalized, the curve depends only on the network's Poisson ratio ν and η_b/η . We have used $\nu = 0.1$ and $\eta_b/\eta = 100$. The two asymptotes given in eq 15 are shown as dashed blue and dotted red lines, with a crossover around $q \sim \lambda^{-1} \ll \xi^{-1}$. The small Poisson ratio, corresponding to an unrealistically compressible network, is chosen to graphically emphasize the difference between the two regimes on a logarithmic scale. For a realistic value of $\nu = 0.4$ we get a difference of about 20%. Equation 15 can be used to calculate the effect for any value of ν . The value of η_b is motivated by the actin networks of ref 16, whose low-frequency response is governed by the viscous term, with viscosity about 100 times that of water.

The second simple limit is where the bare polymer network is taken as purely elastic. In this case $\eta_b = G/(i\omega) + \eta$, and G and K are frequency-independent constants. Substitution in eq 15 and solving for the rate yields

$$G, K = \text{const} : \quad -i\omega = \begin{cases} \Omega_\gamma(q) + \Omega_{\text{el}}, & q \ll \lambda^{-1}, \\ \text{the same, with } \Omega_\gamma \rightarrow \Omega_\gamma \beta^2 / (\beta^2 - 1), & \lambda^{-1} \ll q \ll \xi^{-1}. \end{cases} \quad (17)$$

We have defined here the rates $\Omega_\gamma(q) \equiv \gamma q / (2\eta)$ and $\Omega_{\text{el}} \equiv G/\eta$.

A third limit which can be simply treated is where the bare network's shear modulus has a single-exponential relaxation with some relaxation time τ , $G(\omega) = G_0/(1 + i\omega\tau)$. Once

the frequency dependence of ν is neglected, it is straightforward to obtain from eq 15 the explicit dispersion-relation asymptotes,

$$G = G_0/(1 + i\omega\tau), K = \text{const} : \tag{18}$$

$$-i\omega_{\pm} = \begin{cases} \frac{1}{2} \left[\tau^{-1} + \Omega_{\gamma} \pm \sqrt{(\tau^{-1} + \Omega_{\gamma})^2 - 4\tau^{-1}(\Omega_{\gamma} + \Omega_{\text{el}})} \right], & q \ll \lambda^{-1}, \\ \text{the same, with } \Omega_{\gamma} \rightarrow \Omega_{\gamma}\beta^2/(\beta^2 - 1), & \lambda^{-1} \ll q \ll \xi^{-1}. \end{cases}$$

This relation shows two branches, which may contain an imaginary (oscillatory) component for sufficiently large Ω_{el} .

The dispersion relation of polymer networks was studied previously by Harden et al.^{10–12} That work focused on a different regime, including inertia and restricting the discussion to the strong coupling limit ($\Gamma \rightarrow \infty$ or $\xi \rightarrow 0$). In this limit, the material is a structureless viscoelastic medium. We focus here on structural effects (finite ξ) within the overdamped regime. The two dispersion relations coincide only in one limit, when inertia is taken to zero in refs 10–12, and the bulk limit is taken in our theory ($q \ll \lambda^{-1}$). The experimental conditions under which the present theory is valid will be examined in the Discussion section.

Response to a localized surface force

We consider a point force, $\mathbf{F}\delta(\boldsymbol{\rho})\delta(z)$, applied on the surface of the semi-infinite polymer network at the origin (see Figure 1). Our purpose is to find the resulting surface displacement and flow. This can be viewed as an extension of the elastic Boussinesq problem (ref 3, Section 8) to a viscoelastic material. The equations and boundary conditions are given in the Model section. They are the same as those used to find the dispersion relation in the preceding sub-section, except that now we substitute in the boundary condition of eq 8 a non-zero surface force density, $\mathbf{f} = \mathbf{F}\delta(\boldsymbol{\rho})$. Applying the boundary conditions results in this case in an inhomogeneous set of differential equations, whose solution gives the surface values of the different fields, $\mathbf{u}(\boldsymbol{\rho}, z = 0, \omega)$, $\mathbf{v}(\boldsymbol{\rho}, z = 0, \omega)$, and $p(\boldsymbol{\rho}, z = 0, \omega)$. We focus on the displacement and flow responses, which are captured by a tensor \mathcal{G} ,

$$v_i(\boldsymbol{\rho}, z = 0, \omega) = i\omega u_i(\boldsymbol{\rho}, z = 0, \omega) = \mathcal{G}_{ij}(\boldsymbol{\rho}, \omega)F_j, \tag{19}$$

where summation over repeated indices is used. The first equality follows from the boundary condition of eq 7.

The full expressions in real space could be calculated only numerically. See more details in the supplemental material.⁴⁰ The results are presented in the figures below as solid curves. As in the preceding sub-section, we provide closed-form expressions for the relevant asymptotic limits.⁴⁰ From now on we omit for brevity the mention of $z = 0$ and ω in the arguments of the various functions. In the expressions below, recall that η_b , β , and l_{ec} are in principle all functions of ω .

For the tangential response, \mathcal{G}_{ij} with $i, j = x, y$, we find at large distances,

$$\rho \gg \lambda : \quad \mathcal{G}_{ij}(\boldsymbol{\rho}) = \frac{1}{4\pi\eta_b\rho} \left(\delta_{ij} + \frac{\rho_i\rho_j}{\rho^2} \right). \tag{20}$$

This result coincides with the one obtained in the Boussinesq problem,³ $u_i = (\mathcal{G}_{ij}/i\omega)F_j$, once $i\omega\eta_b$ is replaced by the elastic solid's shear modulus, and the solid is taken as incompressible ($\nu = 1/2$). At shorter distances we find

$$\begin{aligned} \rho \ll \lambda : \quad \mathcal{G}_{ij}(\boldsymbol{\rho}) &= \frac{1}{4\pi\eta_b\rho} \left(A\delta_{ij} + B\frac{\rho_i\rho_j}{\rho^2} \right), \\ A &= \frac{\beta^2\eta_b + \eta}{(\beta^2 - 1)\eta_b + 2\eta}, \\ B &= \frac{(\beta^2 - 2)\eta_b + 3\eta}{(\beta^2 - 1)\eta_b + 2\eta}. \end{aligned} \quad (21)$$

Note that expressions 20 and 21 are independent of the surface tension γ . This is because the surface tension acts as a restoring force in the perpendicular direction only.

From eqs 20 and 21 we derive two results which are particularly relevant for microrheology experiments. The first is the longitudinal response,

$$\rho \gg \lambda, \quad \rho \ll \lambda : \quad \mathcal{G}_L(\rho) = \mathcal{G}_{xx}(\rho\hat{x}) = \frac{1}{2\pi\eta_b\rho}, \quad (22)$$

where we have taken, without loss of generality, the direction connecting the two points as the x axis. Equation 22 corresponds to the case where both the perturbation and the response are aligned with the direction between the two points. The second is the transverse response,

$$\mathcal{G}_T(\rho) = \mathcal{G}_{xx}(\rho\hat{y}) = \mathcal{G}_{yy}(\rho\hat{x}) = \begin{cases} \frac{1}{4\pi\eta_b\rho}, & \rho \gg \lambda, \\ \frac{1}{4\pi\eta_b} \frac{\beta^2\eta_b + \eta}{(\beta^2 - 1)\eta_b + 2\eta} \frac{1}{\rho}, & \rho \ll \lambda, \end{cases} \quad (23)$$

which corresponds to the case where the perturbation and the response are perpendicular to the direction between the points. Having chosen the x axis along that direction, we have $\mathcal{G}_{xy} = 0$ by symmetry. Figure 3 presents the longitudinal and transverse responses as calculated numerically, along with the two asymptotic limits for small and large separations. Note the deviation from the asymptotic behavior at distances $\rho \sim \lambda$, much larger than ξ . We have selected a small value for the Poisson ratio (a highly compressible network) to emphasize that deviation.

We now turn to the perpendicular response $\mathcal{G}_P(\rho) = \mathcal{G}_{zz}(\rho)$, where both perturbation and resulting displacement are perpendicular to the surface. The behavior of this component is richer and affected by the surface tension γ . We find three asymptotic behaviors. At distances larger than both the elastic length λ and the elasto-capillary length l_{ec} we recover again the bulk response,

$$\rho \gg \max(\lambda, l_{ec}) : \quad \mathcal{G}_P(\rho) = \frac{1}{4\pi\eta_b\rho}. \quad (24)$$

This result is independent of both λ and l_{ec} and coincides with the perpendicular response of the Boussinesq problem³ upon the appropriate replacements discussed above. At distances

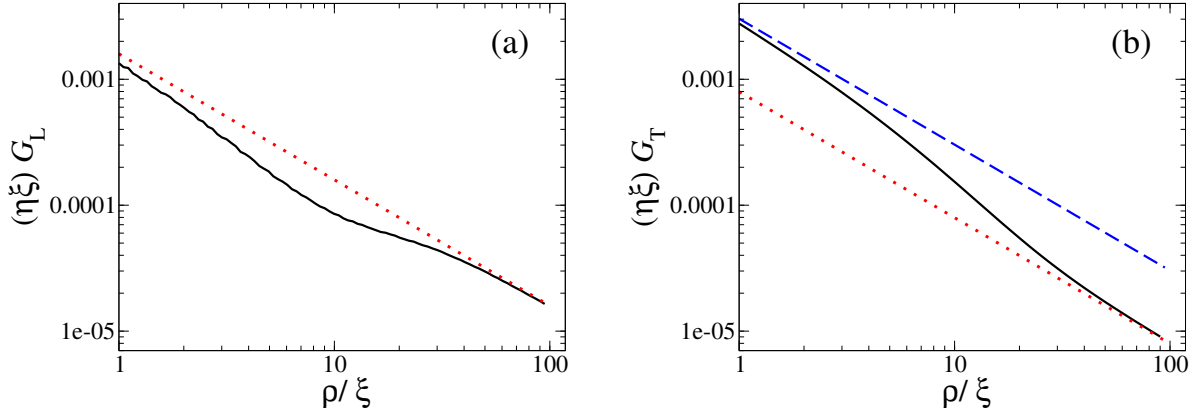


Figure 3: Normalized longitudinal and transverse responses as a function of normalized separation. Once normalized, these functions depend on the parameters ν and η_b/η alone. We have used $\nu = -1$ (in (a)), $\nu = 0.1$ (in (b)), and $\eta_b/\eta = 100$. The curves deviate from their asymptotic limits around $\rho \sim \lambda \gg \xi$. Panel (a) shows the longitudinal response. Numerical results (solid black curve) are shown along with the long- and short-distance asymptote (eq 22; dotted red line). Panel (b) shows the transverse response. Numerical results (solid black curve) are shown along with the large-distance asymptote (dotted red line) and the short-distance one (eq 23; dashed blue line); see . The small Poisson ratios, corresponding to unrealistically compressible networks, are chosen to graphically emphasize the difference between the two regimes on a logarithmic scale. For a realistic value of $\nu = 0.4$ we get a difference of about 2% in (a) and 20% in (b). Equations 22 and 23 can be used to calculate the effect for any value of ν . The value of η_b is motivated by the actin networks of ref 16, whose low-frequency response is governed by the viscous term, with viscosity about 100 times that of water.

much shorter than these length scales, we obtain an effectively two-dimensional, logarithmic response, whose only length scale is l_{ec} ,

$$\rho \ll \min(\lambda, l_{ec}) : \quad \mathcal{G}_P(\rho) = \frac{1}{2\pi\eta_b l_{ec}} \left[\ln\left(\frac{l_{ec}}{\rho}\right) - \gamma_E \right], \quad (25)$$

where $\gamma_E \simeq 0.58$ is Euler's constant. This expression is reminiscent of the flow response of fluid membranes, where the elasto-capillary length plays here the role of the Saffman-Delbrück length, acting as a two-dimensional cutoff.^{41,42} At intermediate distances we find another distinctive regime, which is unaffected by surface tension and depends on the length scale λ (through the Poisson ratio ν),

$$l_{ec} \ll \rho \ll \lambda : \quad \mathcal{G}_P(\rho) = \frac{1}{4\pi\eta_b\rho} \frac{\beta^2}{\beta^2 - 1}. \quad (26)$$

where $\beta(\nu)$ has been defined in eq 16. Figure 4 presents the spatial dependence of \mathcal{G}_P , demonstrating the three asymptotic regimes.

Examining the off-diagonal response $\mathcal{G}_{xz}(\rho)$, we find that it vanishes for all ρ . The xz component vanishes also in the Boussinesq problem when the Poisson ratio is taken to be

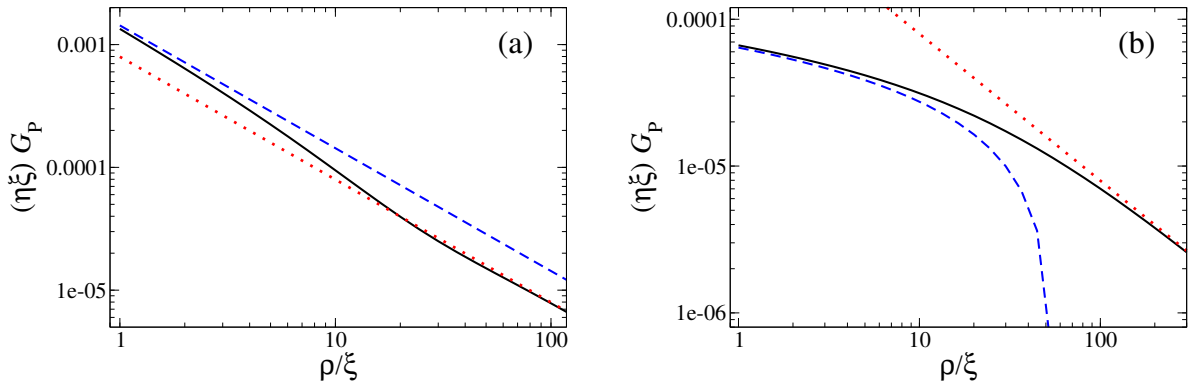


Figure 4: Normalized perpendicular response as a function of normalized separation. Once normalized, these functions depend on the parameters ν , η_b/η and $l_{ec}/\xi = \gamma/(i\omega\eta_b\xi)$. We have used $\nu = 0.1$ and $\eta_b/\eta = 100$. Panel (a) demonstrates the intermediate regime, taking $l_{ec} = 0$ (no surface tension). Numerical results (solid black curve) and the two asymptotes given by eqs 24 (dotted red line) and 26 (dashed blue line) are shown. Panel (b) focuses on the short-distance regime, where we have taken $l_{ec}/\xi = 100$. The numerical result (solid black curve) and the two asymptotes given by eqs 24 (dotted red line) and 25 (dashed blue line) are shown. The small Poisson ratio, corresponding to an unrealistically compressible network, is chosen to graphically emphasize the difference between the two regimes on a logarithmic scale. For a realistic value of $\nu = 0.4$ we get a difference of about 20%. Equations 24–26 can be used to calculate the effect for any value of ν . The value of η_b is motivated by the actin networks of ref 16, whose low-frequency response is governed by the viscous term, with viscosity about 100 times that of water.

$1/2$.³ Thus the vanishing of this component is a result of the overall incompressibility of the medium.

We would like to stress again two points. (a) In all the asymptotic expressions for short distances, eqs 21–23 and 25, the distance ρ must still be kept larger than ξ to ensure the validity of the continuum theory. This is why in all figures we take $\rho/\xi > 1$. (b) We give above the velocity response; to obtain the displacement response one should divide the results for \mathcal{G}_{ij} by $i\omega$ and recall that $i\omega\eta_b = G_b$.

Discussion

Let us summarize the main results which are relevant to experiments. Equation 15 gives the dispersion relation of overdamped surface fluctuations as a function of wavevector in the limits of small and large q , which can be probed by surface scattering. To obtain the explicit decay rate one needs to know the viscoelastic modulus of the specific material. We have demonstrated this procedure for three simple frequency dependencies of the modulus. Conversely, the small- q limit can be used to extract the bulk viscoelastic modulus if the surface tension is known, or vice versa. The main novelty of the present work with respect to surface scattering lies in the crossover between the two asymptotes, occurring for $q \sim \lambda^{-1}$, as well as the large- q asymptote, which depends on the Poisson ratio ν (see Figure 2). These features, which depend on the intrinsic length of the material, have not been considered by earlier theories. For example, they may be used to extract the compression modulus of the bare polymer network. This modulus has eluded measurement, because decoupling it from

the total compression modulus of the medium (which is governed by the solvent’s very large modulus) is hard.¹⁸ The dispersion relation of eq 15 is relevant to low frequencies where inertia is negligible. Comparison with refs 10,11, which included inertial effects, reveals that this requirement is fulfilled for $\omega \ll \min(\sqrt{\gamma q^3/\rho_m}, \eta_b q^2/\rho_m)$, where $\rho_m \sim 1 \text{ gr/cm}^3$ is the medium’s mass density. Checking against eq 15, we find that the dispersion relation is consistent for $q \gg \gamma\rho_m/\eta_b^2$. Thus, the range of validity increases with decreasing surface tension and increasing viscoelasticity. For $\gamma \sim 10 \text{ erg/cm}^2$ and $\eta_b \sim 1 \text{ poise}$, the requirement is $q \gg 10 \text{ cm}^{-1}$ which generally holds. However, at sufficiently large q (i.e., large ω), the bulk viscosity will no longer be much larger than the solvent’s, and the requirement above for ω will not be valid.

Our predictions concerning the response to a localized force are relevant to two-point microrheology.³⁰ Equations 22 and 23 give the longitudinal and transverse velocity responses at the surface. Multiplied by $k_B T/(i\omega)$, they give the correlations between the displacement fluctuations of two tracer particles lying on the surface and separated by a distance ρ , along and transverse to the separation vector, respectively. The results for large separations are found to be equivalent to those for an elastic medium.³ This was experimentally observed for thick films made of hyaluronic acid gels.³² However, once the separation becomes of order λ or less, we expect appreciable deviations from the elastic result (see Figure 3). We note that λ is typically much larger than the mesh size ξ . This prediction, assuming that the experiment covers sufficiently large distances between tracer particles, can be used to measure λ and extract the network’s compression modulus.

In the direction perpendicular to the surface we have found a richer behavior arising from the dependence on the elasto-capillary length. This includes a quasi-two-dimensional membrane-like behavior at small distances (eq 25), and a distinctive intermediate regime which depends on the network’s compressibility (eq 26). Unfortunately, it should be hard to measure displacements perpendicular to the surface at sufficient spatial and temporal resolutions.

The predictions concerning correlations between surface displacements can be used to perform “non-invasive” microrheology, where the viscoelastic moduli of the medium are measured by tracking particles on the surface.^{32–37} Importantly, at sufficiently large distances, this kind of two-point microrheology should be insensitive to surface heterogeneities. It would be insensitive also to features of the particle-surface interactions such as the possible meniscus around the probe particles.

Underlying our results is the assumption of finite friction between network and solvent, which departs from the strong-coupling limit considered earlier.^{10–12} Such friction was found necessary to account for experiments on entangled actin networks.^{16,17} It is expected to occur, in addition, in semi-dilute solutions of long polymers and close to a critical (e.g., theta) point, where the network is highly compressible.

In this work we have highlighted the spatial properties of the surface response. The results can be alternatively discussed from the perspective of frequency dependence. Such a discussion requires detailed knowledge of the viscoelastic properties of the material (i.e., $G_b(\omega)$), which goes beyond the generic theory presented here. In the examples provided above we have assumed the dominance of the viscous contribution at low frequency, as is known for actin networks.¹⁶ In other limits the response would be quite different and its treatment would require specific details. For example, the elasto-capillary length $l_{ec} \sim 1/G_b$, whereas the compressibility length $\lambda \sim \sqrt{G_b/\omega}$. This implies a delicate interplay between the different effects as a function of frequency.

The treatment of a two-fluid boundary could be made more precise in the future. Here we have assumed that the two components move together at the surface (boundary condition

eq 7). Such strong coupling should be valid when both components are strongly repelled from the outer phase, resulting in a sharp interface of large surface tension. To relax this assumption one should replace boundary conditions 7 and 8 by two stress-balance conditions for the two components separately. These conditions would include a friction term proportional to the difference in the surface velocities of the two components. Another assumption behind boundary condition 8 is that the external force is applied to both components. This will be the case in the common microrheology scenario where the force is applied to an inert bead much larger than ξ and in physical contact with both network and solvent. There may be other cases where, for example, the force is applied by a particle bound to the network alone. The same refinement described above would allow also to treat such scenarios. The two stress-balance conditions can include separate external forces for the two components.

The present work has addressed the surface response of an indefinitely thick sample. Considering a film of finite thickness will introduce another length scale, which should lead to even richer behavior. In particular, since many of the results presented here depend on the length λ , which may be orders of magnitude larger than the network's mesh size in the case of low network compressibility, a strong effect of the finite thickness is expected. This will be addressed in a forthcoming publication.

Acknowledgement

This work has been supported by the Israel Science Foundation (Grants No. 164/14 and No. 986/18).

References

- (1) Adamson, A. W.; Gast, A. P. *Physical Chemistry of Surfaces*, 6th ed.; Wiley, 1997.
- (2) de Gennes, P. G.; Brochard-Wyart, F.; Quere, D. *Capillarity and Wetting Phenomena: Drops, Bubbles, Pearls, Waves*, 1st ed.; Springer, New York, 2004.
- (3) Landau, L. D.; Lifshitz, E. M. *Theory of Elasticity*, 3rd ed.; Pergamon press, 1986.
- (4) Cao, B.; Kim, M.; Schaffer, H.; Cummins, H. Surface modes on polymer solutions by surface lightscattering techniques. *J. Chem. Phys.* **1991**, *95*.
- (5) Dorshow, R. B.; Turkevich, L. A. First observation of capillary to Rayleigh mode crossover on the surface of polymer solutions. *Phys. Rev. Lett.* **1993**, *70*, 2439–2442.
- (6) Monroy, F.; Langevin, D. Direct experimental observation of the crossover from capillary to elastic surface waves on soft gels. *Phys. Rev. Lett.* **1998**, *81*, 3167–3170.
- (7) Onodera, Y.; Choi, P.-K. Surface-wave modes on soft gels. *J. Acoust. Soc. Am.* **1998**, *104*, 3358–3363.
- (8) Yoshitake, Y.; Mitani, S.; Sakai, K.; Takagi, K. Surface tension and elasticity of gel studied with laser-induced surface-deformation spectroscopy. *Phys. Rev. E* **2008**, *78*, 041405.
- (9) Monroy, F. Surface hydrodynamics of viscoelastic fluids and soft solids: Surfing bulk rheology on capillary and Rayleigh waves. *Adv. Colloid Interface Sci.* **2017**, *247*.

- (10) Harden, J. L.; Pleiner, H.; Pincus, P. A. A two-fluid model for surface modes on concentrated polymer solutions and gels. *Langmuir* **1989**, *5*, 1436–1438.
- (11) Harden, J. L.; Pleiner, H.; Pincus, P. A. Hydrodynamic surface modes on concentrated polymer solutions and gels. *J. Chem. Phys.* **1991**, *94*, 5208–5221.
- (12) Pleiner, H.; Harden, J. L.; Pincus, P. Surface modes on a viscoelastic medium. *Europhys. Lett.* **1988**, *7*, 383–387.
- (13) Kappler, J.; Shrivastava, S.; Schneider, M.; Netz, R. Nonlinear fractional waves at elastic interfaces. *Phys. Rev. Fluids* **2017**, *2*.
- (14) Wang, C.; Huang, Q. Hydrodynamic surface waves in concentrated polymer solutions in the presence of surface adsorption. *J. Chem. Phys.* **1997**, *107*, 5898–5906.
- (15) Henle, M. L.; Levine, A. J. Capillary wave dynamics on supported viscoelastic films: Single and double layers. *Phys. Rev. E* **2007**, *75*, 021604.
- (16) Sonn-Segev, A.; Bernheim-Groswasser, A.; Diamant, H.; Roichman, Y. Viscoelastic response of a complex fluid at intermediate distances. *Phys. Rev. Lett.* **2014**, *112*, 088301.
- (17) Sonn-Segev, A.; Bernheim-Groswasser, A.; Roichman, Y. Extracting the dynamic correlation length of actin networks from microrheology experiments. *Soft Matter* **2014**, *10*, 83248329.
- (18) Diamant, H. Response of a polymer network to the motion of a rigid sphere. *Eur. Phys. J. E* **2015**, *38*, 32.
- (19) Granek, R.; Diamant, H. Membrane undulations in a structured fluid: Universal dynamics at intermediate length and time scales. *Eur. Phys. J. E* **2018**, *41*, 1.
- (20) Pershan, P. S.; Schlossman, M. L. *Liquid Surfaces and Interfaces: Synchrontron X-rays Methods*; Cambridge University Press, 2012.
- (21) Levine, A. J.; Lubensky, T. C. Response function of a sphere in a viscoelastic two-fluid medium. *Phys. Rev. E* **2001**, *63*, 041510.
- (22) De Gennes, P. G. Dynamics of entangled polymer solutions. I. The Rouse model. *Macromolecules* **1976**, *9*, 587–593.
- (23) De Gennes, P. G. Dynamics of entangled polymer solutions. II. Inclusion of hydrodynamic interactions. *Macromolecules* **1976**, *9*, 594–598.
- (24) Doi, M.; Onuki, A. Dynamic coupling between stress and composition in polymer solutions and blends. *J. Phys. II France* **1992**, *2*, 1631–1656.
- (25) Milner, S. T. Dynamical theory of concentration fluctuations in polymer solutions under shear. *Phys. Rev. E* **1993**, *48*, 3674–3691.
- (26) Bruinsma, R.; Grosberg, A. Y.; Rabin, Y.; Zidovska, A. Chromatin Hydrodynamics. *Biophys. J.* **2014**, *106*, 1871–81.
- (27) Larson, R. G. *The Structure and Rheology of Complex Fluids*; Oxford University Press, New York, 1999.

- (28) Ghaskadvi, R. S.; Dennin, M. A two-dimensional Couette viscometer for Langmuir monolayers. *Rev. Sci. Instr.* **1998**, *69*, 3568–3572.
- (29) Mason, T. G.; Weitz, D. A. Optical measurements of frequency-dependent linear viscoelastic moduli of complex fluids. *Phys. Rev. Lett.* **1995**, *74*, 1250–1253.
- (30) Crocker, J. C.; Valentine, M. T.; Weeks, E. R.; Gisler, T.; Kaplan, P. D.; Yodh, A. G.; Weitz, D. A. Two-point microrheology of inhomogeneous soft materials. *Phys. Rev. Lett.* **2000**, *85*, 888–891.
- (31) Waigh, T. A. Advances in the microrheology of complex fluids. *Rep. Progr. Phys.* **2016**, *79*, 074601.
- (32) Ladam, G.; Vonna, L.; Sackmann, E. Micromechanics of surface-grafted hyaluronic acid gels. *J. Phys. Chem. B* **2003**, *107*, 8965–8971.
- (33) Shlomovitz, R.; Boatwright, T.; Dennin, M.; Levine, A. J. Non-contact microrheology of monolayers and membranes. *Biophys. J.* **2012**, *102*, 34a.
- (34) Shlomovitz, R.; Evans, A. A.; Boatwright, T.; Dennin, M.; Levine, A. J. Measurement of monolayer viscosity using noncontact microrheology. *Phys. Rev. Lett.* **2013**, *110*, 137802.
- (35) Boatwright, T.; Dennin, M.; Shlomovitz, R.; Evans, A. A.; Levine, A. J. Probing interfacial dynamics and mechanics using submerged particle microrheology. II. Experiment. *Phys. Fluids* **2014**, *26*, 071904.
- (36) Komura, S.; Ramachandran, S.; Seki, K. Lateral Dynamics in Polymer-Supported Membranes. *Materials* **2012**, *5*, 1923–1932.
- (37) Komura, S.; Ramachandran, S.; Seki, K. Anomalous lateral diffusion in a viscous membrane surrounded by viscoelastic media. *EPL* **2012**, *97*.
- (38) The solution is much simplified when the equations are decoupled into a collective flow (satisfying the Stokes equation) and a relative flow (satisfying the Brinkman equation). See ref 18.
- (39) Ohmasa, Y.; Yao, M. Surface waves on non-Newtonian viscoelastic liquids. *Phys. Rev. E* **2011**, *83*, 031605.
- (40) See ancillary files.
- (41) Saffman, P. G.; Delbrück, M. Brownian motion in biological membranes. *Proc. Natl. Acad. Sci.* **1975**, *72*, 3111–3113.
- (42) Oppenheimer, N.; Diamant, H. Correlated diffusion of membrane proteins and their effect on membrane viscosity. *Biophys. J.* **2009**, *96*, 3041 – 3049.